doi:10.1006/jmbi.2001.5419 available online at http://www.idealibrary.com on IDEAL® J. Mol. Biol. (2002) 317, 249–262

JMB

Crystal Structure of Yeast Acetohydroxyacid Synthase: A Target for Herbicidal Inhibitors

Siew Siew Pang, Ronald G. Duggleby* and Luke W. Guddat

Centre for Protein Structure Function and Engineering Department of Biochemistry and Molecular Biology, School of Molecular and Microbial Sciences, The University of Queensland, Brisbane QLD 4072, Australia

**Corresponding author*

Acetohydroxyacid synthase (AHAS; EC 4.1.3.18) catalyzes the first step in branched-chain amino acid biosynthesis. The enzyme requires thiamin diphosphate and FAD for activity, but the latter is unexpected, because the reaction involves no oxidation or reduction. Due to its presence in plants, AHAS is a target for sulfonylurea and imidazolinone herbicides. Here, the crystal structure to 2.6 Å resolution of the catalytic subunit of yeast AHAS is reported. The active site is located at the dimer interface and is near the proposed herbicide-binding site. The conformation of FAD and its position in the active site are defined. The structure of AHAS provides a starting point for the rational design of new herbicides.

Keywords: acetohydroxyacid synthase; acetolactate synthase; FAD; thiamin diphosphate; herbicide inhibition

Introduction

The acetohydroxyacid, 2-acetolactate is the precursor of the branched-chain amino acids valine and leucine. It is formed in a reaction catalyzed by acetohydroxyacid synthase (AHAS; EC 4.1.3.18),[1,2] in which pyruvate is decarboxylated and condensed with a second molecule of pyruvate (Figure 1). Isoleucine is formed in a pathway that parallels that of valine biosynthesis, except that AHAS uses pyruvate and 2-ketobutyrate to form 2-aceto-2-hydroxybutyrate.

AHAS, in common with several other enzymes that catalyze the decarboxylation of 2-ketoacids, uses thiamine diphosphate (ThDP) as a cofactor. Such enzymes also require a divalent metal ion that anchors ThDP in the active site. This is demonstrated in the three-dimensional structures of several related enzymes including pyruvate oxidase (POX),[3] pyruvate decarboxylase (PDC),[4–6] and benzoylformate decarboxylase (BFDC).[7] AHAS has an essential requirement for FAD, which is unexpected, because the reaction involves no oxidation or reduction. This has led to speculation[8] that the requirement for FAD is an evolutionary remnant of an ancestral protein, similar to POX, in which FAD played a redox role.

The branched-chain amino acids are not synthesized by animals but are made by microorganisms and plants. This makes AHAS an attractive target for herbicides, and several compounds that are widely used in agriculture act as specific and potent inhibitors of the enzyme.[9] These compounds bear no resemblance to the substrate and are not competitive inhibitors, suggesting that they do not bind at the active site.[10–14] The structure, and natural role, of this herbicide-binding site is unknown, although it has been proposed to be the vestige of a quinone-binding site in an ancestral POX-like enzyme.[11]

The structure of AHAS from any species has not been determined, although homology models have been described.[15,16] Because these models were derived using the experimentally determined structure of POX as a template, they are, necessarily, unable to define accurately any structural details not found in the template. Although these models have been validated to some extent by mutagenesis studies, they are undoubtedly approximate at best. The coordinates of neither model have been published or deposited in the Protein Data Bank.

Previously, we reported the cloning, expression, purification, and characterization of yeast AHAS.[17,18] The enzyme is composed of two types of subunit, the larger of which contains the catalytic machinery and is active alone. Combining this with the smaller regulatory subunit stimulates activity seven- to tenfold and confers sensitivity to

Abbreviations used: AHAS, acetohydroxyacid synthase; ThDP, thiamine diphosphate; POX, pyruvate oxidase; PDC, pyruvate decarboxylase; BFDC, benzoylformate decarboxylase.

E-mail address of the corresponding author: duggleby@biosci.uq.edu.au

0022-2836/02/020249–14 $35.00/0

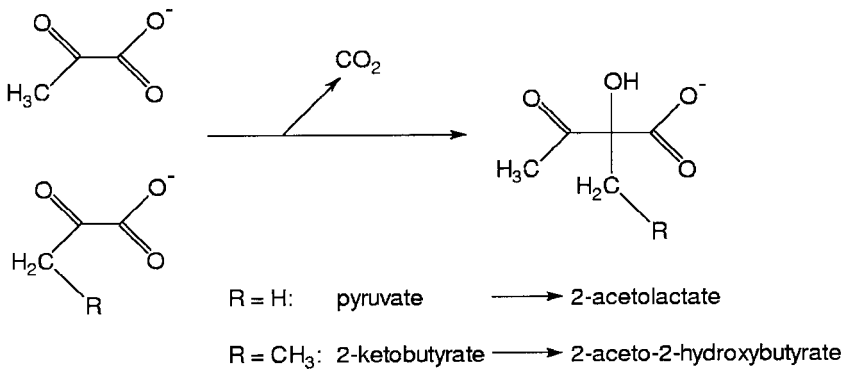

Figure 1. Reactions catalyzed by acetohydroxyacid synthase.

inhibition by valine and activation by MgATP. More recently, we described the crystallization of the catalytic subunit[19] and we now describe the crystal structure of this enzyme at 2.6 Å resolution. This structure reveals the location of several active-site features, including the position and conformation of the cofactors ThDP, Mg^{2+} and FAD. The structure, in combination with molecular modeling, also suggests the geometry and location of the binding site for the imidazolinone herbicide imazapyr (2-(4-isopropyl-4-methyl-5-oxo-2-imidazolin-2-yl)nicotinic acid) and provides the necessary template for future structure-based inhibitor design.

Results and Discussion

Overall structure of the catalytic subunit of yeast AHAS

Crystals of yeast AHAS were grown in the presence of 1 mM ThDP, 1 mM Mg^{2+}, 1 mM FAD and 0.2 M potassium phosphate by hanging-drop vapor diffusion and diffract to 2.6 Å resolution.[19] The crystal structure was solved by molecular replacement using BFDC as a starting model. The R_{factor} and R_{free} for the final structure are 0.188 and 0.219, respectively, and the model has excellent geometry (Table 1). The asymmetric unit in the crystal consists of the polypeptide homodimer, two FAD molecules, two ThDP molecules, two Mg^{2+}, two K^{+}, three phosphate ions and 325 ordered water molecules. A representative electron density map defining the location of FAD is shown in Figure 2(a) and (b).

The protein that was crystallized consists of the mature AHAS protein after removal of the mitochondrial transit peptide (57 residues) plus a 47 residue N-terminal peptide, derived from the pET30 expression plasmid, containing a hexahistidine tag. In the nomenclature employed below, residues are numbered starting at the initiating methionine residue of the precursor protein that includes the mitochondrial targeting sequence. Each monomer has three domains, designated α (85-269), β (281-458) and γ (473-643). For monomer A, no electron density was observed until residue 83, which excludes the entire hexahistidine tag peptide and 26 residues of the mature protein. In addition, no electron density was observed for the last 40 residues of this monomer. The limits of monomer B included one extra residue at each terminus. The overall structure of the homodimer is shown in two different orientations in Figure 3(a) and (b). The two α and two γ-domains form a central core, with one β-domain located on each side of this core.

The average temperature factor for all atoms in the structure is 53.6 $Å^2$. Although this is a high value, it is not unreasonable, given that there are six domains per molecule and there are long flexible polypeptide connectors between the domains. The average temperature factors for the β-domain in monomer B, and to a lesser extent in monomer A, are higher than those for the α and γ-domains (Figure 4). As a result, the overall structure of the

Table 1. Statistics for data collection and refinement

Crystal parameters	
Unit cell length (Å)	$a = 95.6$, $b = 109.4$, $c = 178.9$
Space group	$P2_12_12_1$
Crystal dimensions (mm)	0.5 × 0.2 × 0.2
Diffraction data	
Temperature (K)	100
Resolution range (Å)	50.0-2.6
Observations ($I > 0\sigma(I)$)	214,515 (20,596)
Unique reflections ($I > 0\sigma(I)$)	57,490 (5,733)
Completeness (%)	97.8 (99.2)
R_{sym}[a]	0.058 (0.301)
$\langle I \rangle / \langle \sigma(I) \rangle$	17.1 (3.9)
Refinement	
Resolution limits (Å)	50-2.60
R_{factor}	0.188
R_{free}	0.219
rmsd[b] bond lengths (Å)	0.0064
rmsd bond angles (deg.)	1.274
Ramachandran angles	
Most favored (%)	89.6
Additionally allowed (%)	9.9
Generously allowed (%)	0.4
Disallowed (%)	0.0

[a] $R_{sym} = \Sigma|I - \langle I \rangle| / \Sigma\langle I \rangle$, where I is the intensity of an individual measurement of each reflection and $\langle I \rangle$ is the mean intensity of that reflection. Values in parentheses are statistics for the 2.69-2.60 Å resolution shell.

[b] rmsd, root-mean-square deviation.

protein is somewhat clearer in monomer A, especially in the β-domain. For the most part, the structural descriptions and illustrations presented below are based on monomer A. The exception is in the loop comprising residues 580-595, which is disordered completely in monomer A but traceable in the electron density in monomer B. This region is functionally important for herbicide binding and catalysis, as will be discussed later. Where interactions involve amino acid residues from both monomers, these are distinguished with a prime symbol (′) for those residues from monomer B.

The overall structure of each monomer is similar to that observed in other ThDP-containing enzymes such as BFDC and POX (Figures 5 and 6). The individual domains all have an α-β architecture comprising a central six-stranded parallel β-sheet with several helices surrounding the sheet on both sides (Figure 3(c)). The β-sheets in the α and γ-domains have identical Richardson topology of $1x$, $-2x$, $-1x$, $-2x$, $1x$, while the β-sheet in the β-domain has Richardson topology of -1x, $-1x$, $3x$, $1x$, $1x$. The α-domain has an additional antiparallel β-sheet (two short strands) derived from the N and C-terminal sections of the domain.

There are differences in the overall quaternary structure of several ThDP-dependent enzymes; AHAS and transketolase[20] are dimers, while POX,[3] PDC[4] and BFDC[7] are all tetramers. There are also differences in structure at the subunit level. For example, when the C^{α} atoms of the 356 core residues in monomer A of yeast AHAS are superimposed (Figure 6) on the equivalent C^{α} atoms in BFDC, the rmsd is 1.8 Å, while for POX this value is 2.8 Å. When comparing the equivalent core residues within the three individual domains of the three proteins, the rmsd values vary from 1.2 Å to 1.7 Å. Thus there appears to be little difference in the orientation of the three domains in BFDC *versus* AHAS. However, when POX and AHAS are compared, the β-domains have different orientations relative to the α and γ-domains. A homology model of the structure of *Escherichia coli* AHAS isozyme II has been constructed,[15] using POX as the template. Comparison with the experimental structure of yeast AHAS gave an rmsd of 2.9 Å based on slightly fewer (348) core residues. Thus, yeast AHAS is marginally more similar to POX than it is to the modeled AHAS structure derived from POX.

Active site

AHAS has two active sites, which are on opposite faces of the molecule (Figure 3(a)). Each active site is bordered by amino acid residues from both monomers. In these crystals, the active sites are exposed to solvent, but it is likely that a disordered loop in the γ-domain, a C-terminal extension not observed in this structure, and/or a portion of the regulatory subunit[17] might shield the active site during catalysis.

ThDP-binding site

ThDP is located centrally in the active site (Figure 7) spanning the two monomers. The diphosphate portion of ThDP interacts with Mg^{2+} and with amino acid residues from the γ-domain. The direct contacts (Figure 7(a)) include hydrogen bonds between the phosphate oxygen atoms and the side-chain atoms of His500′, Asp550′, Ser552′ and Asn577′, and the main-chain atoms of Gln499′, His500′, Ala551′ and Ser552′. The two-ring structure of ThDP is secured to the protein by van der Waals contacts (Figure 7(a)) to Tyr113, Gly115, Glu139, Thr162 and Pro165 from one monomer and to Met525′ and Met555′ from the second monomer.

Comparison with other structurally characterized ThDP-dependent enzymes identifies features of the structure of ThDP that are essential for its activation. First, it is bound to AHAS in a V-conformation (Figure 7(c)) as in the other enzymes. The dihedral angles ϕ_T and ϕ_P for ThDP in AHAS are 96° and −66°, respectively, the same values as reported for PDC.[4] The V-conformation is maintained by the side-chain of Met525′, which protrudes from the surface forcing the thiazolium and pyrimidine rings to be bent relative to one another. With ThDP in the V-conformation, a close approach, 3.1 Å, is made between the 4′-amino nitrogen and C2 atoms. Second, there are two conserved hydrogen bonds between the pyrimidine ring and the enzymes. A glutamate residue, corresponding to Glu139 in AHAS, is found in all these enzymes and forms a hydrogen bond to N1′. This completely conserved interaction is suggested to facilitate the formation of the 4′-imino form of ThDP. A second hydrogen bond from the backbone oxygen atom of Gly523′ may stabilize the 4′-amino/imino group and orient it to deprotonate the nearby C2 atom, resulting in the reactive ylide that initiates catalysis. The importance of Glu139 for catalysis has been confirmed by mutagenesis in AHAS[21] and in other ThDP-dependent enzymes.[22–25]

The active site is quite open with the entire thiazolium ring, C4′, N4′, C6, C7 and C7′ fully accessible to solvent. In the crystal structures of other ThDP-dependent enzymes the coenzyme is less accessible, with no more than C2, S1 and N4′ exposed. As mentioned previously, the open structure in AHAS may not reflect the situation during catalysis, where mobile regions could cover the active site. The first of these mobile regions is residues 580-595. Although this loop is traceable in monomer B, it may be confined by crystal packing forces that do not constrain it in monomer A, where it is disordered completely. The termini of this loop are near the active site and we speculate that it may be repositioned during catalysis. Another disordered region is the last 40 residues (39 in monomer B) of the protein. The residues immediately preceding this segment point towards the active site and this

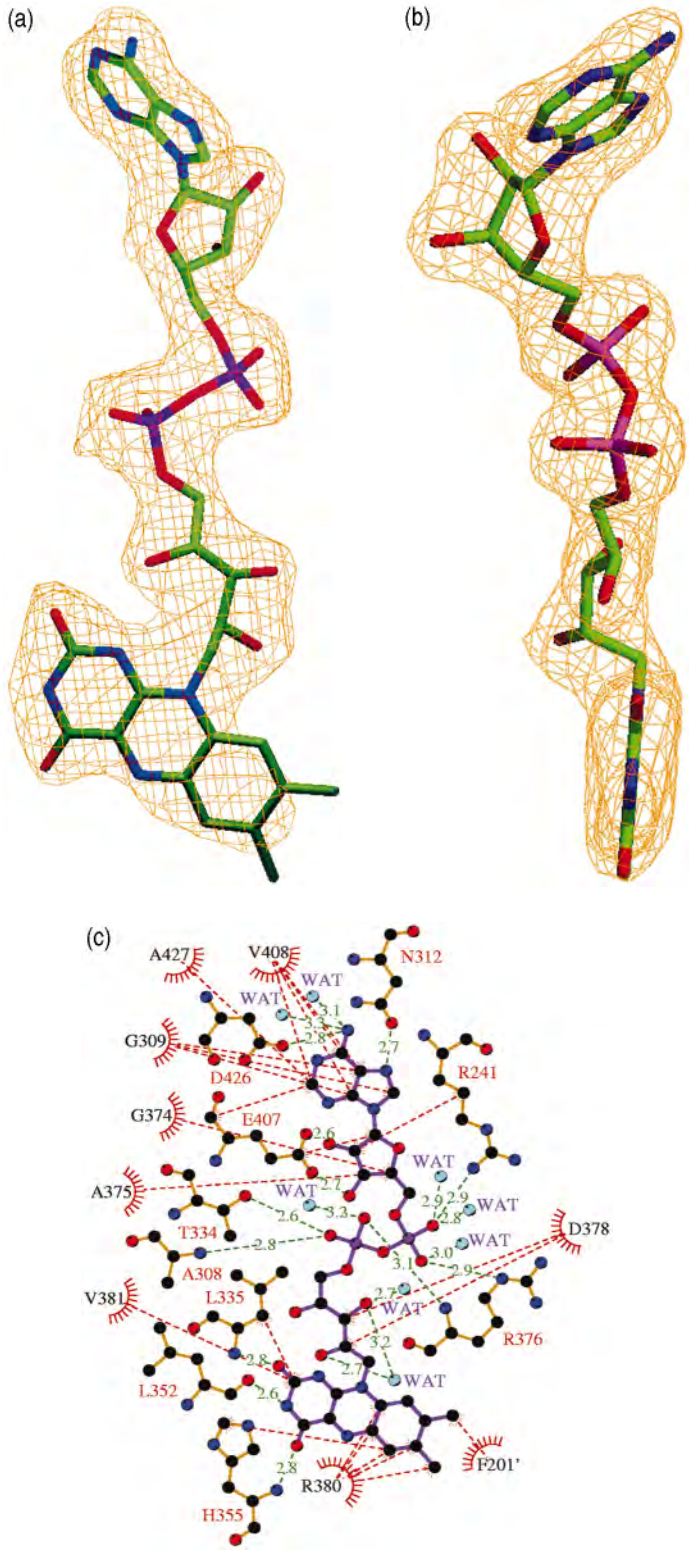

Figure 2. (a) and (b) Orthogonal views of the $2F_o - F_c$ electron density contoured 1σ above the background for the FAD molecule associated with monomer A. (c) A diagram illustrating the residues contacting the FAD molecule associated with monomer A.

disordered part of the protein could form a ''lid'' over the active site. A similar situation has been described in the crystal structures of PDC. The C-terminal region is disordered in the yeast enzyme[4,5] but mostly resolved in *Zymomonas mobilis* PDC.[6] Moreover, deletion of the last nine residues of *Z. mobilis* PDC results in a drastic reduction of activity that is suggested to result from the failure of the active site to close properly during catalysis.[26]

Centered approximately 3.7 Å from C2 of ThDP a prominent, tetrahedrally shaped island of electron density was observed in each monomer. Based on its shape and intensity, together with the composition of the crystallization buffer, we propose that this is a phosphate ion. The oxygen atoms form hydrogen bonds with the main-chain nitrogen atom of Gly116, the side-chain of Gln202 and a water molecule. We speculate that the position of the phosphate ion is that normally occupied by the carboxyl group of pyruvate. A second similar density that we have modeled as a phosphate ion was observed at a dimer interface and near a crystal packing contact. It forms noncovalent interactions with the side-chains of His126 and His599′, and the main-chain nitrogen atom of Thr598′.

FAD-binding site

FAD is bound in an extended conformation and is associated most closely with the β-domain, although it is located in a crevice bounded by all three domains from the same monomer (Figure 3(c)). Yeast AHAS has a K_m value of 0.3 μM for FAD.[27] This high affinity is due to 12 enzyme to FAD hydrogen bonds and numerous van der Waals interactions (Figure 2(c)). Adenine is held tightly to the protein by hydrogen bonds from the 6-amino nitrogen atom and N7 atom to the side-chains of Asp426 and Asn312, respectively. The ribose ring is held in place by hydrogen bonds from the two hydroxyl groups to the side-chain of Glu407. The phosphate groups of FAD form hydrogen bonds with the side-chain and backbone amide nitrogen atom of Arg376, the side-chain oxygen atom of Thr334 and the backbone amide nitrogen atom of Ala308. The phosphate groups are stabilized additionally by hydrogen bonds to four water molecules. The sole interaction with the α-domain of the same monomer is from the side-chain of Arg241 to one of the phosphate oxygen atoms. The flavin forms three hydrogen bonds with the enzyme; these contacts are to the main-chain atoms of Leu335, Leu352 and His355. The flavin also forms numerous van der Waals contacts with Leu335, His355, Arg380 and Val381. An additional hydrophobic contact is formed between the C8 methyl group of the flavin ring and Phe201′ from the second monomer. This is the only contact to the second monomer; thus, the FAD molecule does not appear to play a direct role in stabilization of the dimer interface.

The distance from the flavin ring N5 to C2 of ThDP is 13.3 Å. In addition, the flavin ring is situated such that this nitrogen atom is pointing away from the C2 atom of ThDP (Figure 8). It therefore appears unlikely that the FAD could participate directly in catalysis. However, in POX, the N5 atom of FAD is also distant from the C2 atom of ThDP but in this enzyme FAD clearly has a redox function in the reaction. The route by which electrons are passed from the hydroxyethyl-ThDP intermediate to FAD in POX is unclear but three potential routes have been suggested (Figure 8).[3,28] The first of these is directly to the methyl group on C7 of the flavin moiety, while the second is *via* Phe121′ to C7. We note that in AHAS, Phe201′ occupies a position similar to that of POX Phe121′ (Figure 8). A third, more-favored route[3,28] in POX is *via* Phe479 and the C7 methyl group of the flavin moiety. In AHAS, the corresponding residue in the sequence is Met582 but its location in space is not similar to that of POX Phe479.

One factor that may allow FAD to be redox-active in POX but not in AHAS is that it is planar in AHAS (Figure 2(b)) but bent by 15° across the N5-N10 axis in POX. This bend favors the reduced form and has been described in several flavin-dependent enzymes, although it does not appear to be an absolute requirement for redox function.[29]

The structure does not permit any definite conclusions to be drawn about the possible role of FAD. The distance from C2 of ThDP to the nearest atom of FAD is in excess of 8 Å, making a direct interaction improbable. Certainly, the proposal[30] that an adduct forms between the hydroxyethyl intermediate and the N5 atom of the flavin ring is ruled out unless there is a substantial structural reorganization during catalysis. Overall, we do not think that any active role of FAD in catalysis can be supported.

It has been proposed[8] that FAD is a vestigial remnant reflecting the evolution of AHAS from a POX-like ancestor. This hypothesis relies on the observations that AHAS and POX are similar, and thus related, based on their amino acid sequences, the reactions catalyzed, and their cofactor requirements. The hypothesis can be supported further by comparing the three-dimensional structures of POX and AHAS. These enzymes have very similar secondary structure topology, domain orientation and dimer arrangement. It appears that FAD in AHAS is required solely for structural reasons, maintaining the enzyme active site in the required geometry for catalysis to occur. In this context, we note that there is evidence for a structural role for FAD in POX in addition to its redox function.[31–33] An open question is how the related FAD-independent acetolactate synthase[34] can catalyze the same reaction as AHAS, but is able to function without this cofactor. Presumably, that enzyme has developed new interactions within the polypeptides to maintain the mandatory tertiary and quaternary structure.

Metal ion-binding sites

In common with all other ThDP-dependent enzymes, AHAS requires the presence of a metal ion for activity. In all other ThDP-dependent enzymes the role of the metal ion is the same; it acts as an anchor to hold the ThDP in place by coordinating to two of the phosphate oxygen atoms and two amino acid side-chains. These two

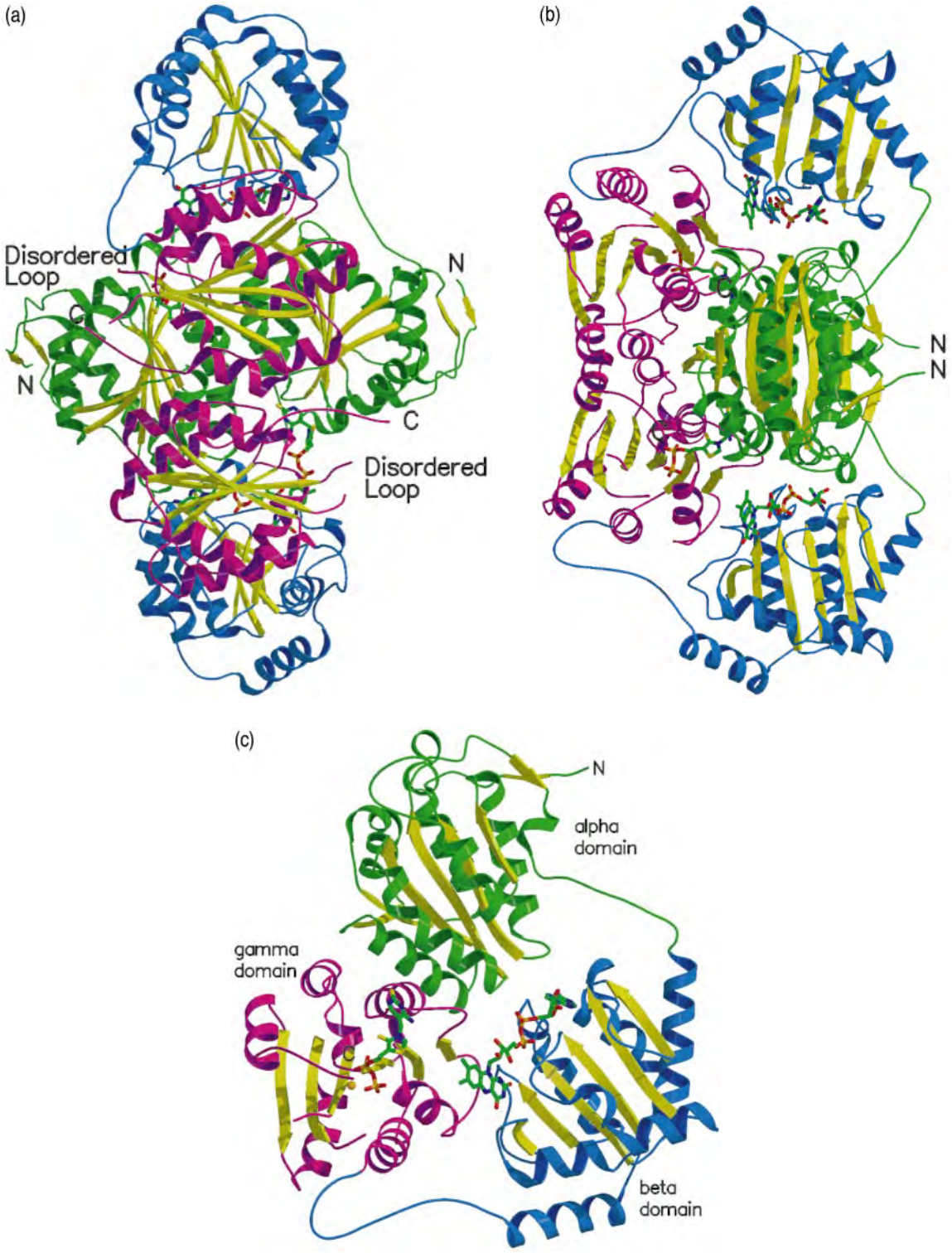

Figure 3. (a) and (b) Orthogonal views of the catalytic subunit of dimeric yeast AHAS. The α-domains are colored green, β-domains blue and γ-domains magenta; β-strands in all domains are colored yellow. FAD and ThDP molecules are depicted as stick models. (c) The structure of monomer A of yeast AHAS. The Mg^{2+} anchored to the ThDP is shown as an orange CPK sphere. A flexible segment joining residues 271 to 279 is not observed in the crystal structure, but has been modeled into the images for completeness.

amino acid residues constitute part of the ThDP binding motif (Figure 5).

In yeast AHAS, we assume that the metal ion is Mg^{2+}, as this was added to the crystallization buffer. The geometry around the metal ion is distorted octahedral (Figure 7(c)). The two phosphate oxygen atoms and the two protein ligands, Asp550′ and Asn577′, form a nearly perfect square plane,

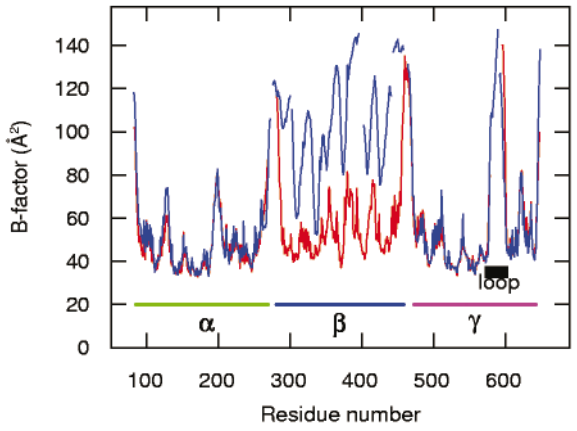

Figure 4. Plot of the *B*-factor, averaged for each atom in a residue, *versus* residue number. Monomer A is shown in red and monomer B in blue. Note the excellent correlation between *B*-factors in the α and γ-domains in the two monomers. Although the *B*-factors in the β-domain of monomer B are elevated compared with monomer A, they correlate well with each other.

while the two water ligands are somewhat displaced from ideal octahedral geometry. The Mg^{2+} coordination is similar to that found in most other ThDP-dependent enzymes, with the two protein ligands representing the second and the last residue of the ThDP motif (Figure 5). It is unusual in ligating to two water molecules; in most related enzymes there is one water molecule only, with the sixth ligand being the backbone oxygen atom of the residue two beyond the end of the ThDP motif (i.e. Glu579′). However, we note that this residue is immediately before a region of high mobility that is disordered completely in monomer A (Figure 4). Thus, we cannot rule out the possibility that in solution, and especially during catalysis, this region might close over the active site with Glu579′ displacing the ligated water molecule. This suggestion is compatible with the structure of the proposed herbicide-binding site that will be described later.

The Mg^{2+} is located near the N-terminal end of helix α17 and there appears to be a second metal ion at the opposite end of this helix (Figure 7(b)) stabilizing the dipole moment. This metal ion is coordinated to the main-chain oxygen atoms of Gln506′ and Trp508′, the side-chain of Gln343′, and to three water molecules. For two reasons, we have assigned this as a potassium ion. Firstly, octahedral geometry is observed, but the distances to the ligand atoms, three protein atoms and three water molecules are in the range 2.7 Å to 3.1 Å, longer than those expected for Mg^{2+}. Secondly, the crystallization solution contains a high concentration of potassium ions and this is the only other metal ion in the crystallization solution.

Herbicide-binding site

AHAS is inhibited by several classes of structurally unrelated compounds.[2] These inhibitors show little resemblance to any of the AHAS substrates, regulators or cofactors, and apparently act as either non-competitive or uncompetitive inhibitors. Two of these classes of compounds are the sulfonylureas and imidazolinones, which are used extensively in agriculture as potent herbicides.[9] Despite the commercial importance of AHAS inhibitors, little is known about the nature and function of the herbicide-binding site or the mechanism of herbicide inhibition. It has been proposed[11] that this site is an evolutionary remnant of the quinone-binding site of a POX-like ancestor. However, the POX structure that has been solved[3,28] is that of an enzyme that uses oxygen rather than a quinone as the electron acceptor. Because of this difference, we are unable to draw any conclusions about the relationship between the herbicide-binding site of AHAS and the quinone-binding site of the proposed POX ancestor.

Identification from mutational studies

A number of bacterial, fungal and plant AHAS variants have been identified that are insensitive to various herbicides. The most extensive series of these is that found in yeast,[35,36] where ten separate mutation sites have been identified (Figure 5). Mutations in AHAS from other species coincide with some of these yeast herbicide-resistance sites and have identified a further five such loci.[2] Almost all of these mutation sites are highly conserved across species in herbicide-sensitive, wild-type AHAS but have no obvious function in catalysis or cofactor binding. These sites extend across all three domains of the protein (Figure 5). Except for the site closest to the C terminus (Gly657), all of these sites can be visualized in either one or both of the monomers. When they are mapped on to the structure, they coalesce into a single region in each dimer interface that defines a plausible herbicide-binding site (Figure 9). The proposed herbicide-binding site is bounded by residues Gly116, Ala117, Leu119, Val191, Pro192, Ser194, Ala200 and Lys251 (α-domain) from one monomer, and Met354′, Asp379′ (β-domain), Met582′, Val583′, Trp586′ and Phe590′ (γ-domain) from the other monomer. This region is quite large at approximately 26 Å × 10 Å and it would be impossible for a herbicide to interact with all of these residues. While it is generally accepted that different classes of herbicide bind to distinct but overlapping sites,[2] the existing inhibitor specificity data suggest that some conformational reorganization of this region will occur. For example, mutation of either Pro192 or Phe590 results in a sulfonylurea-insensitive yeast AHAS[35,36] but these two residues are too distant from one another (Figure 9) to interact simultaneously with the inhibitor. In this context, it may be significant that one boundary of the herbicide-

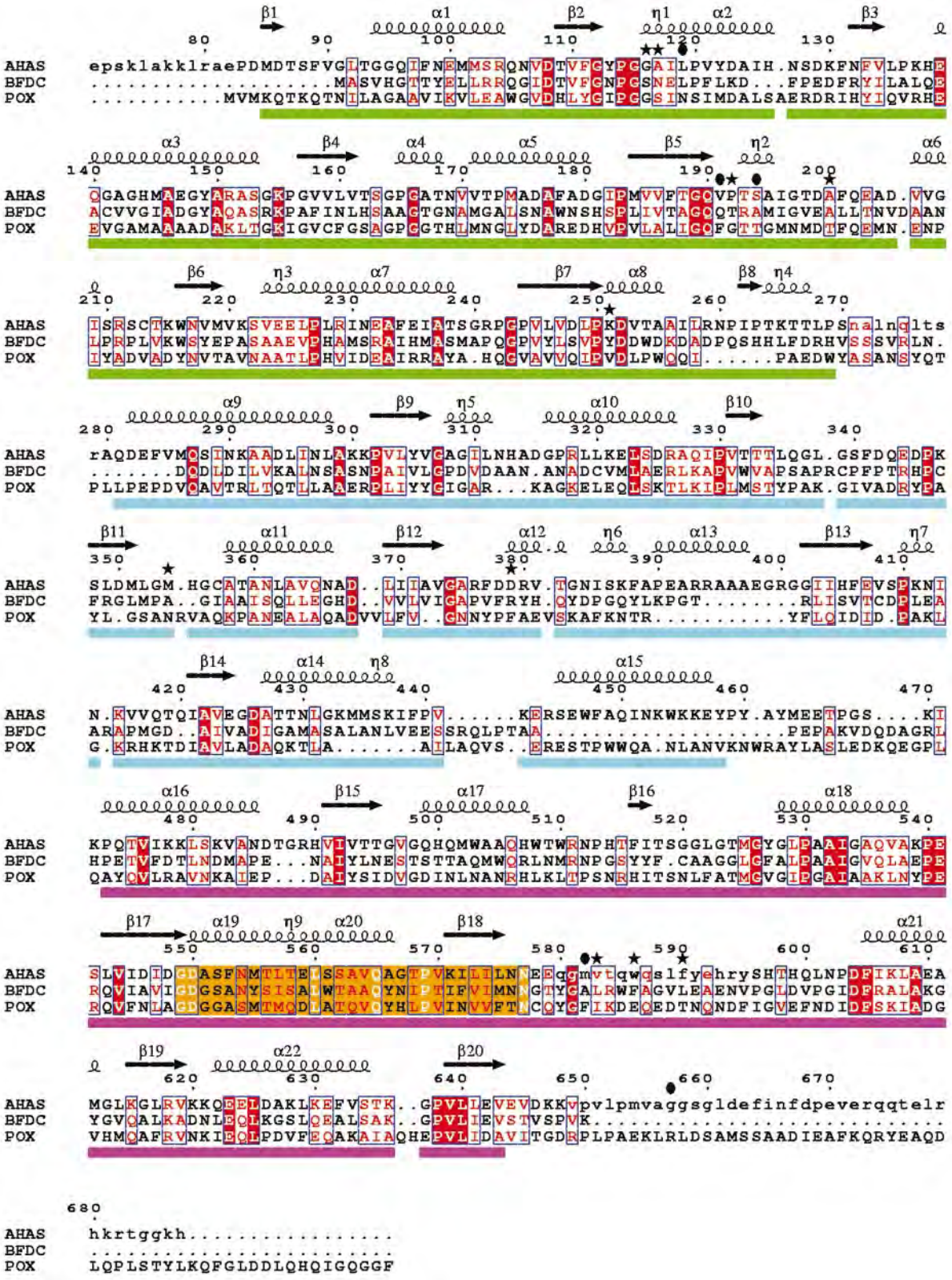

Figure 5. The structure-based sequence alignment of yeast AHAS, BFDC and POX constructed using O[44] and drawn with the program ESPript.[49] The cartoons above the sequences represent α-helices (α1, α2, etc.), β-sheet (β1, β2, etc.) and 3_{10} helices (η1, η2, etc.) in AHAS. The green, blue and purple bars below the sequences represent the α, β and γ-domains of AHAS, respectively, and the orange box encloses the ThDP-binding motif.[50] Residues printed in red are similar between the three sequences, and those printed in white are identical. Residues that, when mutated in yeast, give rise to a herbicidal-resistant AHAS are marked by a star while ovals show the positions of the herbicide-resistance mutations in AHAS from other species. Residues shown in lower-case are not visible in the electron density map of monomer A.

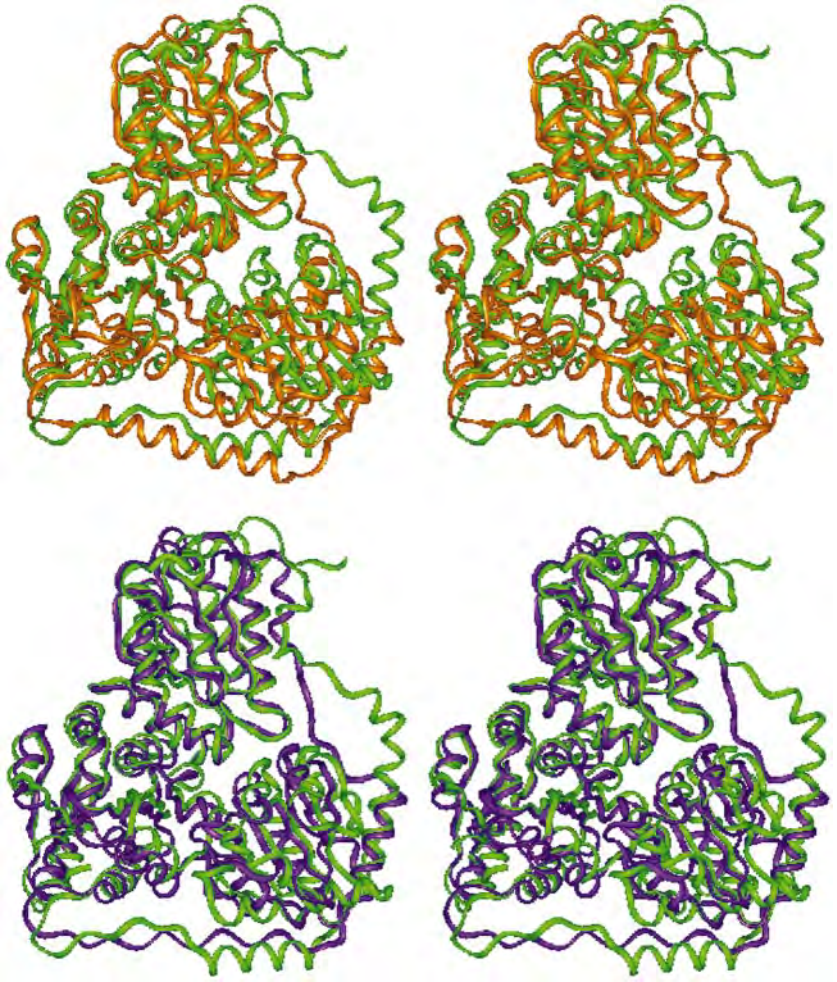

Figure 6. Stereo ribbon diagrams of the structures of AHAS (green), POX (brown) and BFDC (purple). Here, the core C^{α} atoms of the α and γ-domains of the monomers are aligned. The β-domains of AHAS and BFDC are in approximately the same orientation; however, the β-domain of POX is rotated and translated slightly relative to that in AHAS. A flexible segment joining residues 271 to 279 is not observed in the AHAS crystal structure, but has been modeled into the images for completeness.

binding site is defined by the loop that is disordered in monomer A. As mentioned previously, this region might close over the active site during catalysis, producing a more compact herbicide-binding site.

Docking of a herbicidal inhibitor

We have performed docking experiments for the imidazolinone inhibitor imazapyr, using the program GOLD.[37] In this calculation, the herbicide is docked into the proposed herbicide-binding site in a pocket at the dimer interface between the cofactors ThDP and FAD (Figure 9). The nicotinyl ring of imazapyr is 3.5 Å from the thiazolium C2 and overlaps with the position that the active-site phosphate ion occupies in the absence of the herbicide. Given the earlier proposal that the phosphate ion is mimicking the carboxyl group of pyruvate, the docking model implies that imazapyr would impede substrate binding.

Out of the 15 known herbicide-resistance mutations, six (Ala117, Leu119, Pro192, Ser194, Trp586 and Gly657) have been shown to confer imidazolinone-resistance and often cross-resistance to other classes of herbicides.[2] Except for Trp586 (in the mobile loop 580-595) and Gly657 (in the disordered C-terminal region), these imidazolinone-resistance sites interact with, or are in the vicinity of, the herbicide in our docking model (Figure 9). The rest of the sites (Gly116, Val191, Ala200, Lys215, Met354, Asp379, Met582, Val582 and Phe590) have been identified from mutants in which AHAS activity is insensitive to inhibition by sulfonylureas. However, this does not mean that these mutations result in an imidazolinone-sensitive AHAS, since these mutant enzymes have not been tested with such compounds. According to our docking model, most of the herbicide-resistance residues in the α-domain should affect directly the binding of imazapyr. Further studies of the mutant enzymes will be needed to test this prediction and outline the binding sites for the different classes of herbicides.

Active site closure

The mobile loop region (580-595) is near the active site of yeast AHAS. This region is of special interest, since it contains residues that are known

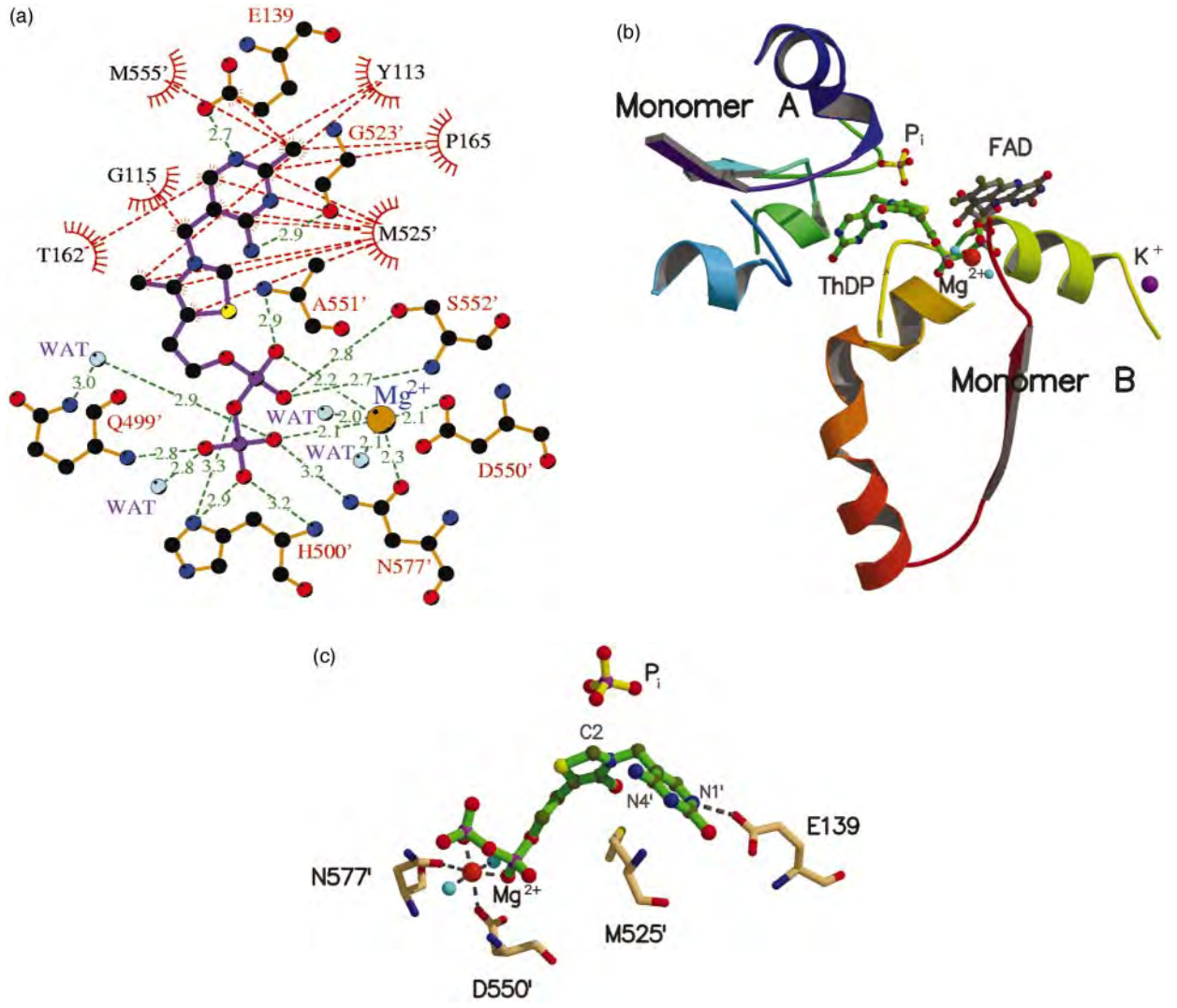

Figure 7. (a) A schematic diagram illustrating the residues contacting the ThDP molecule. (b) View of the active site showing the relative locations of ThDP, Mg^{2+} and the flavin ring of FAD in the dimer interface of yeast AHAS. (c) Contacts between AHAS, ThDP and Mg^{2+}. Coordination distances shown as broken lines to Mg^{2+} are in the range 2.0-2.3 Å.

to be important in substrate specificity[15] (Trp586) and herbicide resistance (Met582, Val583, Trp586 and Phe590). By overlaying the three-dimensional structures of AHAS and other related ThDP-dependent enzymes, the corresponding region has been identified in BFDC (458-473) and POX (477-492). In both enzymes, this loop region is visible, even though it is the most disordered area of BFDC.[7] They are of the same length and show some conservation of sequence when compared to the mobile loop of AHAS (Figure 5). In BFDC and POX, this region forms a helical-loop structure covering the active site of the enzymes. In addition, amino acid residues near the N terminus of this region interact with Mg^{2+} (Thr457 of BFDC; Gln476 of POX) and the diphosphate group of ThDP (Thr457, Gly459 and Ala460 of BFDC; Gly478 and Phe479 of POX), and form weak nonpolar contacts with the thiazole ring of ThDP (Phe479 and Ile480 of POX). In BFDC, this region contains two aromatic amino acid residues (Trp463 and Phe464) that may be involved in substrate specificity.[7] A similar structure is present in PDC but it is four to six amino acid residues shorter than those of AHAS, BFDC and POX. A glutamate residue within this region has been identified to be important in PDC catalysis.[38–40] The mobile loop of AHAS is not folded into any distinct secondary structure and is not within contact distance of the cofactors. These missing interactions are the main reason why ThDP of AHAS is more exposed to solvent as compared to the other enzymes. We propose that during catalysis this loop region and the C-terminal ''lid'' close over the active site, and form direct interactions with reaction intermediates as well with herbicidal inhibitors. Thus, these

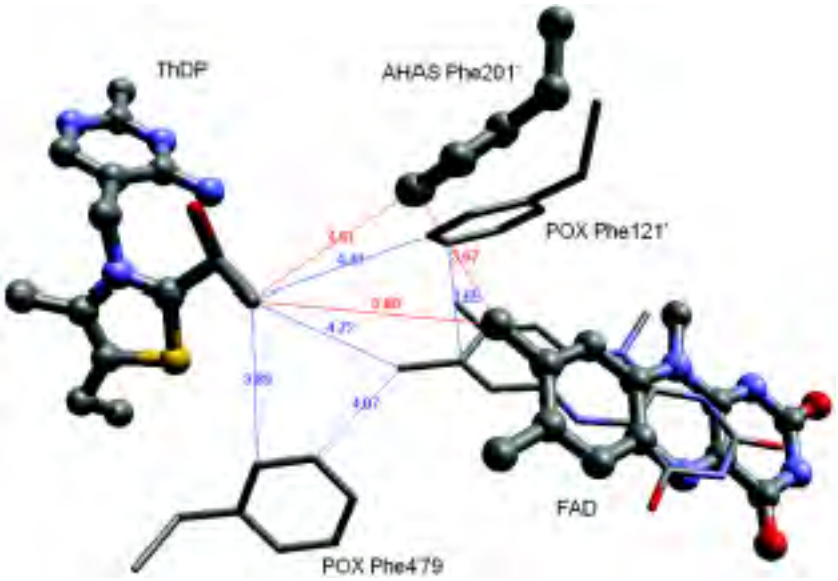

Figure 8. Superposition of the active sites of AHAS and POX. AHAS is shown as a ball and stick model, while POX is depicted as a stick model only. The hydroxyethyl-ThDP intermediate has been modeled in, and shown in blue are the proposed[3,28] routes by which electrons may pass to the FAD in POX. Comparable routes for AHAS are shown in red. Distances are in Å. Carbon atoms are colored gray, oxygen red, nitrogen blue and sulfur yellow.

regions may become ordered and visible in crystal structures of AHAS plus reaction intermediate analogs or herbicides.

Conclusions

The position, conformation, and environment of ThDP in AHAS are similar to those found in homologous enzymes. The FAD appears to be too far from ThDP to participate directly in catalysis, although its position is similar to that found in POX. The location of the herbicide-binding site was inferred from the positions of residues that, when mutated, result in a herbicide-insensitive AHAS. These mutations are found throughout the length of the protein but coalesce into a single region at the subunit interface in the folded protein. The active site is located at the subunit interface and is near the proposed herbicide-binding site.

The yeast AHAS structure provides the framework to solve the closely related structures of AHAS from plants and bacteria, and for solving the structure of the complex between the catalytic and regulatory subunits.[17] Future research is directed at obtaining crystals of this multi-subunit complex as well as those with bound substrate analogs, regulatory effectors[18] (valine and MgATP), and herbicides. The structure of the catalytic subunit of AHAS provides the architecture to understand the molecular basis for herbicide-resistance data and for the mode of binding of the herbicides themselves.

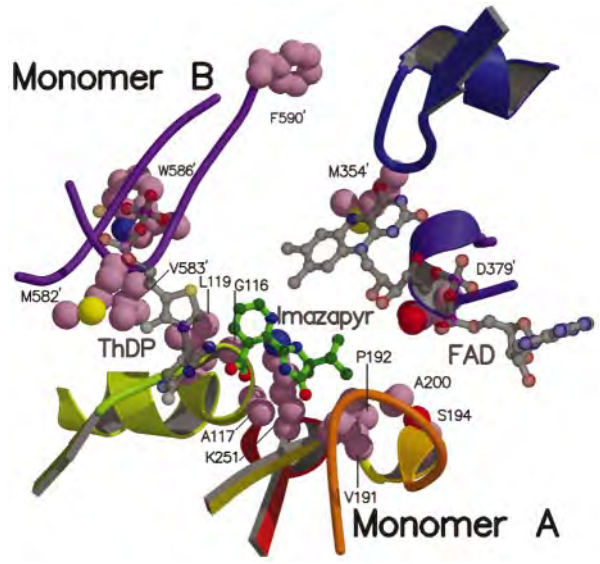

Figure 9. Proposed interaction of AHAS and the herbicidal inhibitor, imazapyr, which was docked into the enzyme using the program GOLD.[37] Amino acid residues at herbicide-resistance sites are labeled and shown as CPK models.

Materials and Methods

Expression, purification, crystallization and X-ray data collection

The catalytic subunit of *S. cerevisiae* AHAS was expressed, purified and crystallized as described.[17,19] X-ray data (Table 1) were collected from cryoprotected crystals at 100 K on Beam Line 14C at the Advance Photon Source in the Argonne National Laboratory, Chicago, USA. The data were indexed, integrated and scaled using the programs DENZO and SCALEPACK.[41]

Structure determination

The crystal structure was solved by molecular replacement using the program AMoRe.[42] A monomeric model consisting of residues 9-161 (α-domain) and 382-521 (γ-domain) from BFDC produced two independent

peaks in the rotation search and translation function. Combining these two peaks resulted in a plausible dimeric structure with acceptable crystal packing contacts. Since the sequence similarity for AHAS is higher for POX than BFDC, the coordinates of POX, including the β-domain, were superimposed onto the BFDC solution and these coordinates were used as the starting point for refinement. Rigid-body refinement was performed with CNS,[43] which reduced the R_{factor} from 0.542 to 0.524 for the data between 6 and 4 Å resolution. This structural model was checked against the initial 2.6 Å resolution $2F_o - F_c$ electron density map using the program O.[44] Amino acid residues or polypeptide segments that fitted poorly were omitted prior to annealing refinement. All subsequent rounds of model building and refinement were carried out using O and CNS. In the initial stages of refinement, strict non-crystallographic symmetry restraints were employed. During the later stages of refinement it became clear that structural differences existed between the two β-domains in the asymmetric unit, and for some loops in the α and γ-domains. As a result, the non-crystallographic restraints were released for those regions. This resulted in a reduction of the R_{free} value from 0.27 to 0.23. Individual *B*-factors were assigned for all atoms and an overall anisotropic *B*-factor correction was applied using the standard protocol in CNS. The final model consists of residues 83-270, 280-579 and 596-648 from monomer A, residues 82-272, 276-300, 302-396, 403-441, 444-458, 464-590 and 592-649 from monomer B, two FAD molecules, two ThDP molecules, two Mg^{2+}, two K^+, three phosphate ions and 325 ordered water molecules. Data collection and refinement statistics are shown in Table 1. Figures were generated with LIGPLOT,[45] SETOR,[46] MOLSCRIPT,[47] Raster3D,[48] WebLab ViewerPro (MSI, San Diego, CA), ESPript[49] and INSIGHT98 (MSI, San Diego, CA).

Docking of imazapyr to the active site of AHAS

A three-dimensional model of imazapyr was constructed using the SKETCHER module of INSIGHT98. The center of the docking site was defined as the point midway between the ThDP and FAD. The docking calculations were limited to a radius of 10 Å from the center of the docking site. Three independent docking runs gave coordinates for imazapyr that, when all of the atoms were superimposed, had an rmsd of less than 0.2 Å.

Coordinates

The coordinates and structure factors of AHAS have been deposited with the RCSB Protein Data Bank under accession number 1JSC.

Acknowledgments

This work was supported by grants from the Australian Research Council to R.G.D. and L.W.G. Coordinates of the *E. coli* AHAS isozyme II homology model[15] were kindly provided by David Chipman, Ben-Gurion University, Israel. We thank Harry Tong, Gary Navrotski and Wilfried Schildkamp for assistance at beam line 14C, Advanced Photon Source, Argonne National Laboratory, Chicago, USA. The use of the BioCARS sector was supported by the Australian Synchrotron Research Program, which is funded by the Commonwealth of Australia under the Major National Research Facilities Program. Use of the Advanced Photon Source was supported by the US Department of Energy, Basic Energy Sciences, Office of Energy Research. Some X-ray data were collected with the assistance of Michael Lawrence at CSIRO in Parkville, Australia.

References

1. Chipman, D., Barak, Z. & Schloss, J. V. (1998). Biosynthesis of 2-aceto-2-hydroxy acids: acetolactate synthases and acetohydroxyacid synthases. *Biochim. Biophys. Acta*, **1385**, 401-419.
2. Duggleby, R. G. & Pang, S. S. (2000). Acetohydroxyacid synthase. *J. Biochem. Mol. Biol.* **33**, 1-36.
3. Muller, Y. A. & Schulz, G. E. (1993). Structure of the thiamine- and flavin-dependent enzyme pyruvate oxidase. *Science*, **259**, 965-967.
4. Dyda, F., Furey, W., Swaminathan, S., Sax, M., Farrenkopf, B. & Jordan, F. (1993). Catalytic centers in the thiamin diphosphate dependent enzyme pyruvate decarboxylase at 2.4-Å resolution. *Biochemistry*, **32**, 6165-6170.
5. Arjunan, P., Umland, T., Dyda, F., Swaminathan, S., Furey, W., Sax, M. *et al*. (1996). Crystal structure of the thiamin diphosphate-dependent enzyme pyruvate decarboxylase from yeast *Saccharromyces cerevisiae* at 2.3 Å resolution. *J. Mol. Biol.* **256**, 590-600.
6. Dobritzsch, D., König, S., Schneider, G. & Lu, G. (1998). High resolution crystal structure of pyruvate decarboxylase from *Zymomonas mobilis*. Implications for substrate activation in pyruvate decarboxylases. *J. Biol. Chem.* **273**, 20196-20204.
7. Hasson, M. S., Muscate, A., McLeish, M. J., Polovnikova, L. S., Gerlt, J. A., Kenyon, G. L. *et al*. (1998). The crystal structure of benzoylformate decarboxylase at 1.6 Å resolution: diversity of catalytic residues in thiamin diphosphate-dependent enzymes. *Biochemistry*, **37**, 9918-9930.
8. Chang, Y.-Y. & Cronan, J. E., Jr (1988). Common ancestry of *Escherichia coli* pyruvate oxidase and the acetohydroxy acid synthases of the branched-chain amino acid biosynthetic pathway. *J. Bacteriol.* **170**, 3937-3945.
9. Shaner, D. L. & Singh, B. K. (1997). Acetohydroxyacid synthase inhibitors. In *Herbicide Activity: Toxicology, Biochemistry and Molecular Biology* (Roe, R. M., Burton, J. D. & Kuhr, R. J., eds), pp. 69-110, IOS Press, Amsterdam, The Netherlands.
10. Shaner, D. L., Anderson, P. C. & Stidham, M. A. (1984). Imidazolinones: potent inhibitors of acetohydroxyacid synthase. *Plant Physiol.* **76**, 545-546.
11. Schloss, J. V., Ciskanik, L. M. & Van Dyk, D. E. (1988). Origin of the herbicide binding site of acetolactate synthase. *Nature*, **331**, 360-362.
12. Durner, J. & Böger, P. (1991). New aspects on inhibition of plant acetolactate synthase by chlorsulfuron and imazaquin. *Plant Physiol.* **95**, 1144-1149.
13. Hill, C. M., Pang, S. S. & Duggleby, R. G. (1997). Purification of *Escherichia coli* acetohydroxyacid synthase isozyme II and reconstitution of active enzyme from its individual pure subunits. *Biochem. J.* **327**, 891-898.
14. Chang, A. K. & Duggleby, R. G. (1997). Expression, purification and characterization of *Arabidopsis thaliana* acetohydroxyacid synthase. *Biochem. J.* **327**, 161-169.

15. Ibdah, M., Bar-Ilan, A., Livnah, O., Schloss, J. V., Barak, Z. & Chipman, D. M. (1996). Homology modeling of the structure of bacterial acetohydroxy acid synthase and examination of the active site by site-directed mutagenesis. *Biochemistry,* **35**, 16282-16291.
16. Ott, K. H., Kwagh, J. G., Stockton, G. W., Sidorov, V. & Kakefuda, G. (1996). Rational molecular design and genetic engineering of herbicide resistant crops by structure modeling and site-directed mutagenesis of acetohydroxyacid synthase. *J. Mol. Biol.* **263**, 359-368.
17. Pang, S. S. & Duggleby, R. G. (1999). Expression, purification, characterization and reconstitution of the large and small subunits of yeast acetohydroxyacid synthase. *Biochemistry,* **38**, 5222-5231.
18. Pang, S. S. & Duggleby, R. G. (2001). Regulation of yeast acetohydroxyacid synthase by valine and ATP. *Biochem. J.* **357**, 749-757.
19. Pang, S. S., Guddat, L. W. & Duggleby, R. G. (2001). Crystallization of the catalytic subunit of *Saccharomyces cerevisiae* acetohydroxyacid synthase. *Acta Crystallog. sect. D,* **57**, 1321-1323.
20. Lindqvist, Y., Schneider, G., Ermler, U. & Sundström, M. (1992). Three-dimensional structure of transketolase, a thiamine diphosphate dependent enzyme, at 2.5 Å resolution. *EMBO J.* **11**, 2373-2379.
21. Bar-Ilan, A., Balan, V., Tittmann, K., Golbik, R., Vyazmensky, M., Hübner, G. *et al*. (2001). Binding and activation of thiamin diphosphate in acetohydroxyacid synthase. *Biochemistry,* **40**, 11946-11954.
22. Wikner, C., Meshalkina, L., Nilsson, U., Nikkola, M., Lindqvist, Y., Sundström, M. & Schneider, G. (1994). Analysis of an invariant cofactor-protein interaction in thiamin diphosphate-dependent enzymes by site-directed mutagenesis - glutamic-acid-418 in transketolase is essential for catalysis. *J. Biol. Chem.* **269**, 32144-32150.
23. Candy, J. M., Koga, J., Nixon, P. F. & Duggleby, R. G. (1996). The role of residues glutamate-50 and phenylalanine-496 in *Zymomonas mobilis* pyruvate decarboxylase. *Biochem. J.* **315**, 745-751.
24. Killenberg-Jabs, M., König, S., Eberhardt, I., Hohmann, S. & Hübner, G. (1997). Role of Glu51 for cofactor binding and catalytic activity in pyruvate decarboxylase from yeast studied by site-directed mutagenesis. *Biochemistry,* **36**, 1900-1905.
25. Fang, R., Nixon, P. F. & Duggleby, R. G. (1998). Identification of the catalytic glutamate in the E1 component of human pyruvate dehydrogenase. *FEBS Letters,* **437**, 273-277.
26. Chang, A. K., Nixon, P. F. & Duggleby, R. G. (2000). Effects of deletions at the carboxyl terminus of *Zymomonas mobilis* pyruvate decarboxylase on the kinetic properties and substrate specificity. *Biochemistry,* **39**, 9430-9437.
27. Poulsen, C. & Stougaard, P. (1989). Purification and properties of *Saccharomyces cerevisiae* acetolactate synthase from recombinant *Escherichia coli*. *Eur. J. Biochem.* **185**, 433-439.
28. Muller, Y. A., Schumacher, G., Rudolph, R. & Schulz, G. E. (1994). The refined structures of a stabilized mutant and of wild-type pyruvate oxidase from *Lactobacillus plantarum*. *J. Mol. Biol.* **237**, 315-335.
29. Fraaije, M. W. & Mattevi, A. (2000). Flavoenzymes: diverse catalysts with recurrent features. *Trends Biochem. Sci.* **25**, 126-132.
30. Schloss, J. V. & Aulabaugh, A. (1988). Acetolactate synthase and ketol-acid reductoisomerase: a search for a reason and a reason for a search. In *Biosynthesis of Branched Chain Amino Acids* (Barak, Z., Chipman, D. M. & Schloss, J. V., eds), pp. 329-356, VCH Press, Weinheim, Germany.
31. Risse, B., Stempfer, G., Rudolph, R., Möllering, H. & Jaenicke, R. (1992). Stability and reconstitution of pyruvate oxidase from *Lactobacillus plantarum*: dissection of the stabilizing effects of coenzyme binding and subunit interactions. *Protein Sci.* **1**, 1699-1709.
32. Bertagnolli, B. L. & Hager, L. P. (1993). Role of flavin in acetoin production by two bacterial pyruvate oxidases. *Arch. Biochem. Biophys.* **300**, 364-371.
33. Tittmann, K., Proske, D., Spinka, M., Ghisla, S., Rudolph, R., Hübner, G. & Gunther, K. (1998). Activation of thiamin diphosphate and FAD in the phosphate-dependent pyruvate oxidase from *Lactobacillus plantarum*. *J. Biol. Chem.* **273**, 12929-12934.
34. Störmer, F. C. (1968). The pH 6 acetolactate-forming enzyme from *Aerobacter aerogenes*. II. Evidence that it is not a flavoprotein. *J. Biol. Chem.* **243**, 3740-3741.
35. Falco, S. C., McDevitt, R. E., Chui, C.-F., Hartnett, M. E., Knowlton, S., Mauvais, C. J. *et al*. (1989). Engineering herbicide-resistant acetolactate synthase. *Dev. Ind. Microbiol.* **30**, 187-194.
36. Mazur, B. J. & Falco, S. C. (1989). The development of herbicide resistant crops. *Annu. Rev. Plant Physiol. Plant Mol. Biol.* **40**, 441-470.
37. Jones, G., Willett, P., Glen, R. C., Leach, A. R. & Taylor, R. (1997). Development and validation of a genetic algorithm for flexible docking. *J. Mol. Biol.* **267**, 727-748.
38. Chang, A. K., Nixon, P. F. & Duggleby, R. G. (1999). Aspartate-27 and glutamate-473 are involved in catalysis by *Zymomonas mobilis* pyruvate decarboxylase. *Biochem. J.* **339**, 255-260.
39. Huang, C.-Y., Chang, A. K., Nixon, P. F. & Duggleby, R. G. (2001). Site-directed mutagenesis of the ionizable groups in the active site of *Zymomonas mobilis* pyruvate decarboxylase: effect on activity and pH dependence. *Eur. J. Biochem.* **268**, 3558-3565.
40. Sergienko, E. A. & Jordan, F. (2001). Catalytic acid-base groups in yeast pyruvate decarboxylase. 2. Insights into the specific roles of D28 and E477 from the rates and stereospecificity of formation of carboligase side products. *Biochemistry,* **40**, 7369-7381.
41. Otwinowski, Z. & Minor, W. (1997). Processing of X-ray diffraction data collected in oscillation mode. *Methods Enzymol.* **276**, 307-326.
42. Navaza, J. (1994). AMoRe: an automated package for molecular replacement. *Acta Crystallog. sect. A,* **50**, 157-163.
43. Brünger, A. T., Adams, P. D., Clore, G. M., Delano, W. L., Gros, P., Grosse-Kunstleve, R. W. *et al*. (1998). Crystallography and NMR System (CNS): a new software system for macromolecular structure determination. *Acta Crystallog. sect. D,* **54**, 905-921.
44. Jones, T. A., Zou, J. Y., Cowan, S. W. & Kjeldgaard, M. (1991). Improved methods for building protein models in electron density maps and the location of errors in these models. *Acta Crystallog. sect. A,* **47**, 110-119.
45. Wallace, A. C., Laskowski, R. A. & Thornton, J. M. (1995). LIGPLOT: a program to generate schematic diagrams of protein-ligand interactions. *Protein Eng.* **8**, 127-134.
46. Evans, S. V. (1993). SETOR: hardware lighted three dimensional solid model representations of macromolecules. *J. Mol. Graph.* **11**, 134-138.

47. Kraulis, P. J. (1991). MOLSCRIPT - a program to produce both detailed and schematic plots of protein structures. *J. Appl. Crystallog.* **24**, 946-950.
48. Merritt, E. A. & Murphy, M. E. P. (1994). Raster3D version 2.01: a program for photorealistic molecular graphics. *Acta Crystallog. sect. D,* **50**, 869-873.
49. Gouet, P., Courcelle, E., Stuart, D. I. & Metoz, F. (1999). ESPript: analysis of multiple sequence alignments in PostScript. *Bioinformatics,* **15**, 305-308.
50. Hawkins, C. F., Borges, A. & Perham, R. N. (1989). A common structural motif in thiamin pyrophosphate-binding enzymes. *FEBS Letters,* **255**, 77-82.

Edited by R. Huber

(Received 26 September 2001; received in revised form 19 December 2001; accepted 22 December 2001)